SEMARAK ILMU PUBLISHING

Journal of Advanced Research in Applied Sciences and Engineering Technology

Journal homepage:
https://semarakilmu.com.my/journals/index.php/applied_sciences_eng_tech/index
ISSN: 2462-1943

Mechanical Characterisation of 3D-Printed Porous PLA Scaffolds with Complex Microarchitectures for Bone Tissue Engineering Applications

Akbar Teguh Prakoso[1,2], Ardiansyah Syahrom[3,4], Amir Arifin[2], Hasan Basri[2,*]

[1] Engineering Science, Faculty of Engineering, Universitas Sriwijaya, Palembang 30139, South Sumatera, Indonesia
[2] Department of Mechanical Engineering, Faculty of Engineering, Universitas Sriwijaya, Kabupaten Ogan Ilir, Palembang, Sumatera Selatan, Indonesia
[3] Applied Mechanics and Design, School of Mechanical Engineering, Faculty of Engineering, Universiti Teknologi Malaysia (UTM), 81410 Johor Bahru, Malaysia
[4] Medical Devices and Technology Centre (MEDITEC), Institute of Human Centred and Engineering (iHumEn), Universiti Teknologi Malaysia (UTM), 81310 Johor Bahru, Malaysia

ARTICLE INFO

Article history:
Received 13 August 2023
Received in revised form 2 March 2024
Accepted 15 May 2024
Available online 15 June 2024

Keywords:
Porous scaffolds; mechanical properties; FEM; tortuosity

ABSTRACT

Bone transplantation remains the leading approach in addressing orthopaedic trauma or disease. In cases where this option is not viable, bone tissue engineering offers an alternative through the use of scaffolding. This approach involves the removal of damaged bone tissue and its replacement with porous scaffold structures to support the regeneration process. Recently, additive manufacturing has emerged as a promising technology for producing scaffold structures that satisfy the necessary performance criteria. In this study, PLA scaffolds with tortuous pore network designs were fabricated using fused deposition modelling. Scaffolds were fabricated with four different porosity values by changing the pore diameter in the range of 840–1732 µm. Sixteen specimens were tested under monotonic compression testing. Result shows the elastic moduli generated by each sample with 25%, 45%, 60% and 75% porosity: 545.21 ± 109.76, 446.82 ± 57.12, 312.55 ± 82.64 and 123.81 ± 23.95 MPa, respectively. Finite element simulation showed good correlation with experimental results, thereby effectively assessing the scaffold mechanical behaviour. Accordingly, the proposed finite element model can predict the mechanical behaviour of fabricated bone scaffolds accurately. The results demonstrate that the numerically predicted elastic modulus of complex scaffold is not closer to experimental outcomes in comparison with as-built samples. Overall, these findings suggest the potential of 3D-printed PLA scaffolds with tuneable porosity for cancellous bone replacement applications.

1. Introduction

Tissue engineering (TE) scaffolds apply the principles of biology and engineering to the development of functional substitutes for bone defects, such as caused by osteonecrosis, cancer and severe traumatic injuries [1-5]. In orthopaedic application, TE scaffold is implanted directly into the injured site, then the body's self-healing mechanism is integrated, inducing bone tissue regenerations

* *Corresponding author.*
E-mail address: hasan_basri@unsri.ac.id

https://doi.org/10.37934/araset.47.1.3955

in-vivo. One of the major challenges in tissue engineering scaffold development is optimizing scaffold design to satisfy biological requirements. The scaffold's design should consider its structure, including factors, such as tortuosity, porosity, shape, pore size, specific surface area and surface curvature. These factors are important because they affect nutrient transport and mechanical integrity as well as new bone formation [6-9]. For example, scaffolds with tortuous microchannel promote better cell attachment during tissue growth and permeability than scaffold with relatively straight microchannels [10]. Porosity, pore size and shape also improve implant mechanical interlocking and provide better mechanical stability [11-13]. The mechanical behaviour of the porous scaffold, in a particular modulus elasticity, is necessary to provide sufficient mechanical support to facilitate bone regeneration [14]. Modulus stiffness of the implanted scaffold should be matched with the surrounding bone tissue to acquire longevity by averting so-called stress shielding, depending on the material used to support bone regeneration [15,16]. Ideal modulus stiffness of scaffold closely matches that of cancellous bone and falls within the range of 0.01 GPa to 2 GPa [17-19].

Recently, the additive manufacturing (AM) technology, especially fused deposition modelling (FDM) is believed to be the most convenient approach to construct 3D porous scaffold with the elaborated geometry and pore structure. FDM technology allows a close control of scaffold design geometry with higher reproducibility, better accuracy and relatively lower production costs than other AM, such as stereolithography (SLA), selective laser sintering (SLS) and selective laser melting (SLM) [20-22]. The wide range of applications for FDM in the porous scaffold fabrication has been expanded by the biocompatibility of lactic acid-based polymers, such as poly-lactic acid (PLA) [23-25]. The conclusions suggest that PLA material is promising for use in orthopaedic implants, as evidenced by the successful formation of apatite on the surface of PLA scaffolds in vitro test subjects with basic lattice structures [26].

In recent years, many research efforts have been dedicated to microarchitecture complete design types and the manufacture of PLA scaffold and its composite using FDM technique. Grid structure is the simplest and most widely used structure in bone scaffolds. The geometry can be produced by depositing parallel filaments in one layer, prior to changing filament orientation on sequential layers [27-31]. The most common orientation schemes or raster angles are 0°/90°, 0°/60°/120°, orthogonal (2xOrtho), staggered orthogonal (2xSt-Ortho), isometric (2xIso) and staggered isometric (2xSt-Iso). Baptista and Guedes [31] investigated the morphological and mechanical behaviour of PLA scaffold depending on raster angle and layer configuration. The morphology of scaffold especially porosity, pore size and connectivity were adjusted by changing the filament offset. However, its pore connection and permeability are unsatisfactory, negatively influencing the continuous growth of cells and tissue [32,33]. Moreover, many stress concentrations at the intersection nodes of the Grid scaffold adversely affect its mechanical performance [34]. Triply periodic minimal surface (TPMS) structure has attracted considerable attention in various fields as a new type of porous structure [35,36]. In terms of the structural design of scaffold, the structural characteristic of TPMS, including pore size, shape and porosity can be controlled by adjusting the parameter to simulate the porous structure of natural bone. Therefore, TPMS may be an ideal and convenient porous structure design method for constructing bone scaffold models. On one hand, the TPMS structure has excellent pore connectivity, permeability, high specific surface area and outstanding tortuosity [37]. Thus, it can effectively simulate the natural bone structure and benefit the cell migration, proliferation and differentiation on the scaffold. On the contrary, the TPMS structure has an interconnected and smooth porous structure, which is beneficial for relieving stress concentration and improving the mechanical performance of the scaffold. However, TPMS structure is difficult to controllable given its morphology, such as porosity, pore size, tortuosity and its graded structure, using advanced

mathematical equations [38]. While the role of scaffold morphology has been considered necessary in bone replacement design, the importance of tortuosity has yet to be further elaborated.

Many studies have been conducted on cell attachment, proliferation, and differentiation in tissue scaffolds and collective cell migration behavior, somewhat influenced by tortuous design parameters. Cell migration efficiency in scaffolds with tortuous architecture provides superior cell attachment compared to scaffolds having relatively straight microchannels [10]. The geometric curvature of the scaffold is thought to play an important role in the migration of tortuous microchannel cells in promoting bone tissue regeneration. Modifying the surface curve where cells connect to the extracellular matrix will promote tissue development [39,40]. Mazalan *et al.,* [41] established a tortuous microchannel device from polydimethylsiloxane (PDMS) to investigate collective cell migration under various geometric constraints, with a tortuosity index ranging from 1.57 to 2.30. The authors found that changing the radius of curvature and the tortuosity index resulted in a unique collective cell migration speed.

Although tortuosity is directly related to permeability, the direct relationship between tortuosity parameter and the mechanical strength of scaffold structures has not been previously demonstrated, warranting further investigation. This study hypothesis that tortuosity can be influenced by altering the pore size and radius of the curvature, which in turn enhances porosity and reduces the cross-sectional area and modulus stiffness. Furthermore, the specific surface area may play a role in this approach. The objective of this study is to investigate mechanical behavior of tortuous scaffold model using experimental and computer simulations.

2. Methodology

2.1 Material

Commercial transparent PLA material for 3D printing was acquired from ESUN in the form of Ø 1.75 mm filament and density of 1.24 g/mm^3. The spool was conditioned in a humidity-controlled environment.

2.2 Scaffold Design

In this study, the scaffold is an open porous model with tortuous microchannel made with SolidWorks (Dassault systems SolidWorks Corp., Waltham, MA, USA) software. A schematic of the scaffold design stage is shown in Figure 1. Initially, pore shape was generated using meandering pore channel concepts with parametric design as shown in Table 1. The radius curvature of the pore channel was set to 0.9 mm. The unit cell of scaffold, namely, Negative Schwarz Primitive (NSP) was generated using Boolean subtraction function with the primary dimension of width, height and length measuring "4.2×4.2×4.2 mm", respectively. The unit cell was considered with four different porosities Φ (25%, 45%, 60% and 75%) within the porosity range of the cancellous bone structure [42,43]. The unit cell of scaffold was stacked to create scaffold architecture. Finally, cylindrical scaffold model was created with diameter 8 mm and height 12 mm. Each geometry was labelled after the structure and its porosity; for example, NSP25r0.9 refers to the Negative Schwarz Primitive scaffold with Φ: 25% porosity and radius curvature 0.9 mm. The final scaffold's porosity and tortuosity can be modified at convenience by changing the fluid pore dimension (X) and radius curvature (r).

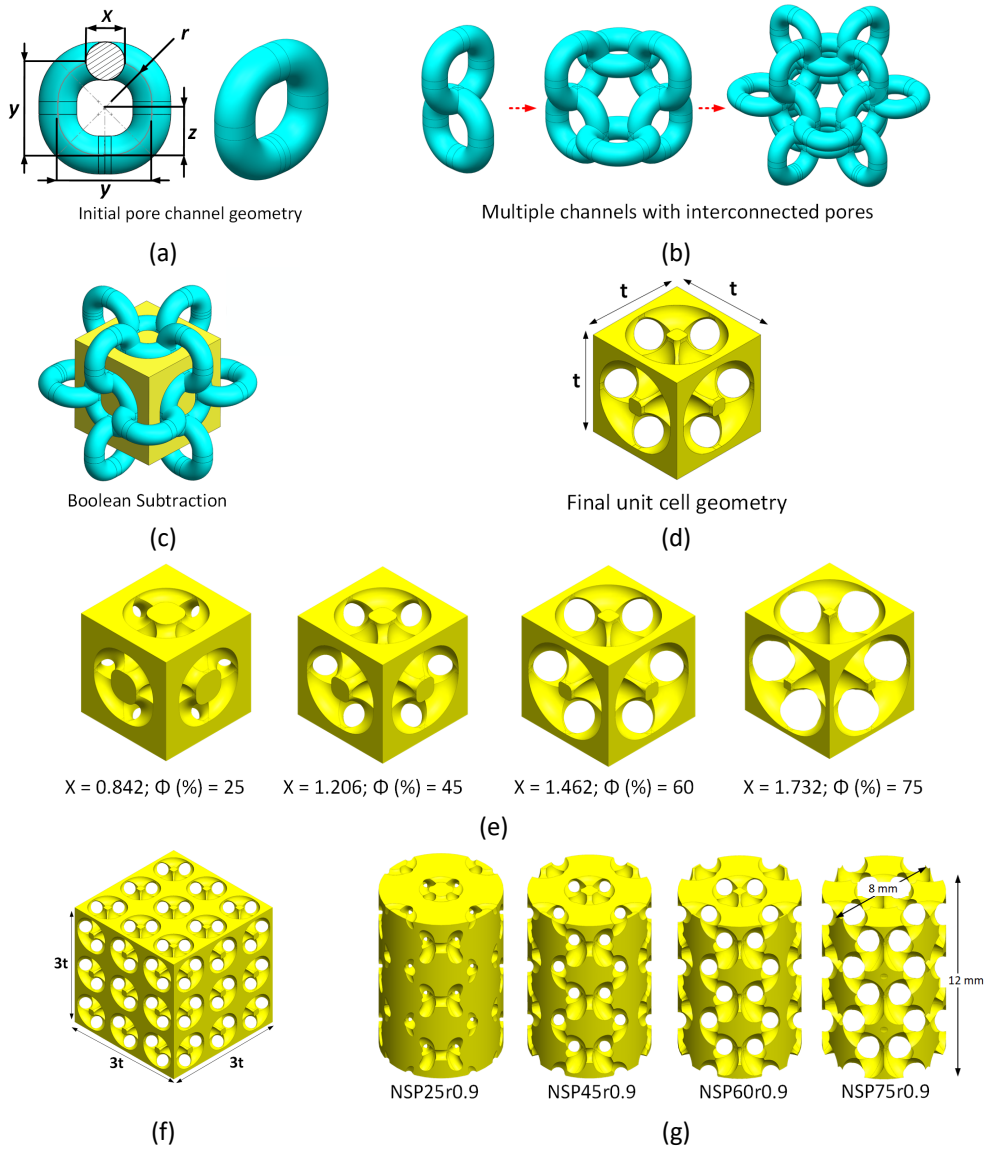

Fig. 1. Schematic process showing the unit cell design principle based on tortuosity fluid pathway. (a) Fluid channel geometry. (b) Following the geometry duplication and assembly, they are interconnected to create tortuous fluid pathway. (c) The fluid geometry and a solid cubic was assembled. (d) 3D model was obtained by Boolean subtraction function. (e) Unit cell porosity controlled by tuning up the fluid pore size and radius curvature. (f) assembled Unit cell of scaffold. (g) Modelled scaffold specimen

Table 1
Dimension parameter features of the Negative Schwarz Primitive (NSP) model CAD design (see also Figure 1)

Dimensional parametric study	Value (mm)		
Model	NSPr0.8	NSPr0.9	NSPr0.98
r	0.8	0.9	0.98
constant, c	1.49	1.49	1.49
y	$2c - r$	$2c - r$	$2c - r$
z	$c - \frac{r}{2}$	$c - \frac{r}{2}$	$c - \frac{r}{2}$
t	4.2	4.2	4.2
x (Φ : 25%)	0.9	0.842	0.82
x (Φ : 45%)	1.24	1.206	1.2
x (Φ : 60%)	1.48	1.462	1.464
x (Φ : 75%)	N/A	1.732	1.752

NSPr0.8 = NSP scaffold model with radius curvature of 0.8 mm; NSPr0.9 = NSP scaffold model with radius curvature of 0.9 mm; NSPr0.98 = NSP scaffold model with radius curvature of 0.98 mm.

2.3 Morphological Analysis

The unit cell of scaffold morphology, including porosity and surface area, was conducted using CAD software features. 3D CAD models were exported to stereolithography (STL) format and imported into the slice software program Chitubox (CBD-Tech, Guangdong, China). The CAD model was sliced using resolution of 17.20 µm. The remaining 244 slices and 500 x 500-pixel images were analysed using Fiji (Image J, NIH). The image data set was then exported to MATLAB (MathWorks Corp., Natick, MA, USA) software to calculate the diffusion tortuosity. The open solver plugin Taufactor is used to calculate the tortuosity value based on the finite difference method (FDM), and image voxels are directly used as discretisation meshes for simulation [44,45].

2.4 Scaffold Fabrication

The designed specimen was sliced using CURA software to generate G-code files. The fabrication parameter is listed in Table 2 according previous literature, and approximately 1 hour is required for each sample to complete [31,46,47]. Four identical specimens for each porosity group were additively manufactured. The scaffold was fabricated using low-cost Creality Ender 3 3D printer. In fabricating the complete 3D structure with material extrusion, the nozzle is heated to melt the filament prior to layer-by-layer deposition. The prepared specimens are shown in Figure 2. The samples have a few manufacturing imperfections, but the overall structure is intact.

Table 2
Fabrication Process

Parameter	PLA
Extruder temperature	210°C
Bed temperature	60°C
Nozzle diameter	0.2 mm
Printing speed	25 mm/s
Layer thickness	0.08 mm
Support type	Brim
Nozzle size	0.2 mm

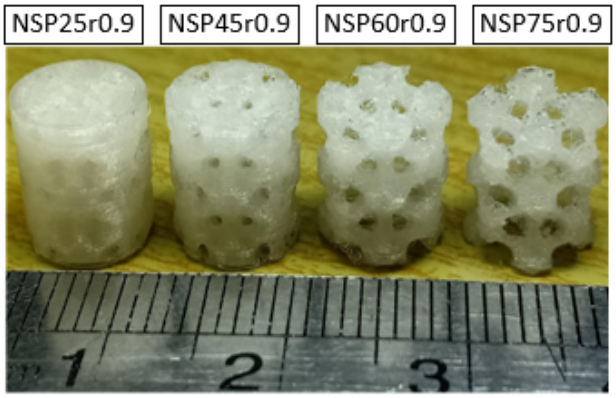

Fig. 2. Fabricated PLA scaffolds

2.5 Material Characterization

PLA scaffold was characterised by scanning electron microscopy (SEM). The Archimedes method in ethanol was used to determine the density of printed scaffold; these values were used to calculate the effective scaffold's porosity. Axia Chemi SEM (Thermo Fisher Scientific, Waltham, MA, USA) was used to study the morphology, porosity and defect features of the produced PLA scaffolds prior to mechanical testing.

2.6 Experimental Compression Test

Compression tests were performed to evaluate the mechanical properties of PLA scaffolds. The test was carried out at the crosshead speed of 0.001 min/min using universal testing machine (The Fast Track 8874, Instron, Norwood, USA). The procedure was determined as per ASTM D1621 and ASTM D695 standard. The compression characteristic including quasi-elastic gradient and compression test were calculated from the stress–strain curve. The quasi-elastic gradient is defined as the slope of the straight line at the beginning of the compression stress–strain curve, which is defined as the modulus of elasticity. The yield stress was measured as a compression offset stress of 0.2%. Monotonic compression test (n = 4) was carried out upon all scaffold's configurations, i.e., porosity 25%–75%. The compressive stress is also recorded and measured. The experimental setup is shown in Figure 3.

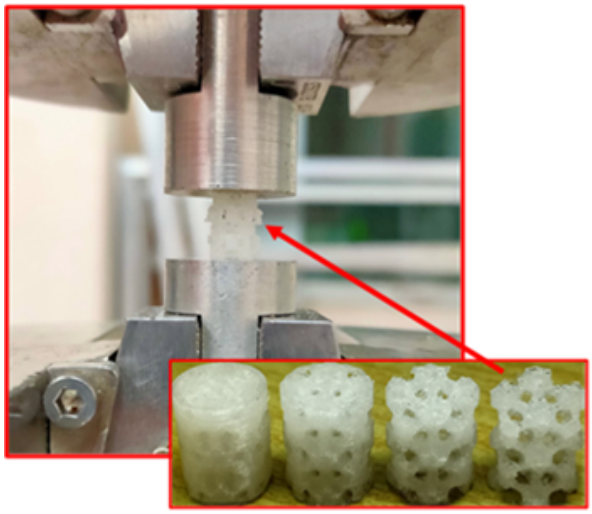

Fig. 3. Isometric views with vertical applied load

2.7 Numerical Analysis

Finite element analysis (FEA) was carried out using COMSOL Multiphysics software to identify the mechanical properties and failure mechanism of the structures [48]. Prior to the FEA analysis, pure solid PLA samples (n = 4) were compressed to determine the material properties including elastic modulus, yield strength and plastic strain. Using standard equation, namely, Eq. (1) and Eq. (2), the nominal yield strain and nominal plastic strain produced by the experiments were converted to true stress and strain. The true stress and strain were determined to identify the plasticity behaviour under similar loading conditions in the finite element model.

$$\varepsilon_{true} = \ln(1 + \varepsilon_{nom}) \tag{1}$$

$$\sigma_{true} = \sigma_{nom}(1 + \varepsilon_{nom}) \tag{2}$$

where σ_{true} indicates true stress, ε_{true} is true strain, σ_{nom} represents nominal stress, and ε_{nom} is nominal strain.

Furthermore, CAD models of similar size to the fabricated model were used to simulate and validate the experimental test. The elastic properties of PLA were assigned to achieve a modulus of 1350 MPa and a density 1250 kg/m^3. The value of elastic modulus obtained from the experimental work is reasonable, ranging from 1 GPa to 4 GPa. Poisson's ratio was set to 0.36. The 3D model of porous PLA was assigned homogenous, isotropic and elastic–plastic properties. The boundary conditions are demonstrated in Figure 4, where time-dependent displacement boundary condition refers to the nodes assigned on the top surface to be solved in a finite domain. In addition, a zero-displacement boundary condition was assigned to the opposite surface in its normal direction, simulating a stationary compression platen. Nodes included in this boundary condition were confined only in the y-direction but were to move freely inside the x–z plane. The macroscopic compression strain limit of 30% was selected for the scope of this study because plasticity is predicted to occur within the specified plastic strain range.

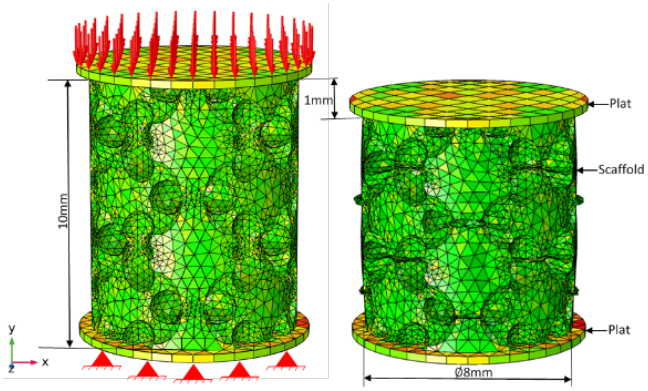

Fig. 4. Isometric views with boundary condition for compression test

2.8 Convergence Mesh Method

The u is the parameter for the mesh sensitivity test using the grid convergency index (GCI) analysis [49]. An example of GCI calculation is

$$GCI = F_s \left| \frac{1}{u_{finer}} \frac{u_{finest} - u_{finer}}{r_{ff}{}^{q_n - 1}} \right| \cdot 100\% \quad (3)$$

F_s is safety factor of 1.25, r is the grid refinement ratio, and q is the convergency observed order. The numerical calculation of q is

$$q_{n+1} = ln \left| \left(\frac{u_{fine} - u_{finer}}{u_{finer} - u_{finest}} \left(r_{fsfr}{}^{q_n - 1} \right) \right) + r_{fsfr}{}^{q_n} \right| / \ln \left(r_{fsfr} \cdot r_{frf} \right) \quad (4)$$

And for the r calculation is

$$r_{ff} = \left(\frac{M_{finer}}{M_{finest}} \right)^{0.5} \quad (5)$$

M is the mesh number. Then, the mesh number is normalized by inverse comparison. The example of normalized mesh number (h) is

$$h_{finest} = h_{finer} \cdot r_{ff} \quad (6)$$

Where h_{finer} of 1. The u_{exact} or $u_{\Delta x \to \sim}$ or is predicted using the extrapolation approach. The formulation for extrapolation is

$$u_{\Delta x \to \sim} = u_{finer} - \left(\frac{u_{finest} - u_{finer}}{r_{ff}{}^{q_{n+1} - 1}} \right) \quad (7)$$

3. Results and Discussion

A new design scaffold with tortuous pore parameters was considered. Scaffolds with pore tortuous have proven to have a promising topological structure that mimics the natural cancellous bone. Adequate mechanical properties are provided for structural strength and biological properties to permit tissue ingrowth, especially for load-bearing applications. Maintaining a high-strength scaffold with sufficient stiffness is crucial to avoid bone loosening and stress shielding effect between the scaffold and surrounding tissue. Therefore, the significant parameters to consider are porosity, pore size and tortuosity. Compression tests have been conducted to evaluate the mechanical characteristics of all specimens. An experimental test was performed to validate the result from the FEA. Notably, FEA was much easier to deform severely due to smooth and frictionless contact between the specimen and the platen during the compression process. The bond strength between layers should be improved to achieve a 3D-printed complex structure, such as NSP, through fused deposition modelling with excellent mechanical properties. In this regard, the process parameters should be optimized [50,51]. Applying optimized parameters in 3D printing leads to the production of scaffold with acceptable mechanical properties [52].

3.1 GCI Calculation Result

Four mesh numbers are compared to find out the optimum mesh number: 40k (coarse), 61.2k (medium), 115k (fine), 759.8k (finest). Based on the calculation using Eq. (5) and Eq. (6), the h_{fs} is 1, h_f is 2.57, h_m is 3.52, h_c is 4.35 respectively. Based on FEA results, the E of each mesh is 780.38 MPa

(coarse), 720.06 MPa (medium), 661.33 (fine), 660.18 MPa (finest). Furthermore, based on Eq. (4), the q_n of 13.82. Then, using Eq. (7), the exact value from the extrapolation approach using 3rd orded polynomial was 659.81 MPa. Finally, using Eq. (3) the GCI_{fsf} of 0.06%, the GCI_{fm} of 11.99%, and the GCI_{mc} of 19.42%. Therefore, the mesh number of 115k was chosen since, based on GCI results has an error below 1%. A summary of the GCI calculation results can be seen in Figure 5.

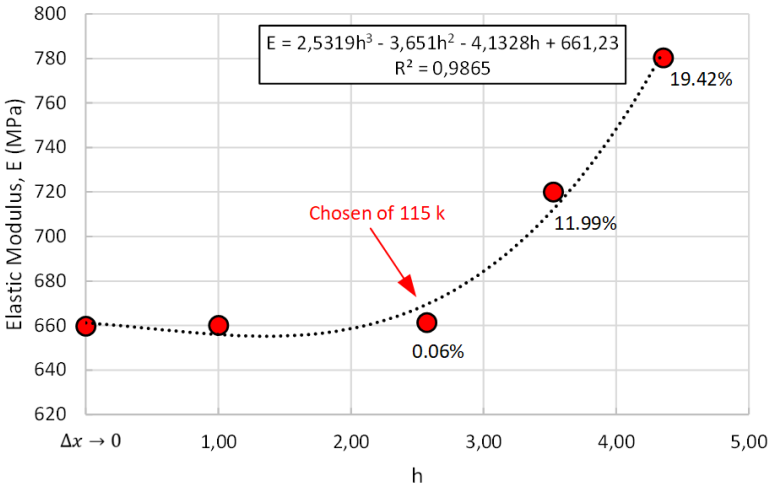

Fig. 5. Mesh sensitivity study on NSP scaffold

3.2 Mechanical Characterization

Monotonic compression tests using experimentation and simulation were carried out on the produced PLA scaffold specimen. The monotonic stress–strain compression curve of the porous scaffold with Φ: 25% porosity is shown in Figure 6(a). PLA scaffold showed elastic deformation in the initial stage, then a long plateau up to the strain of 0.04 in the plastic deformation stage, followed by densification deformation. Meanwhile, the curve shows good agreement between experimental and simulation data for strains up to 0.005. The simulation curve gradually increased (known as the plateau region) past the 0.03 strain. This phenomenon is caused by the consideration of only the yield strength of the material acquired from the experimental data using the FE software.

Furthermore, the scaffold's porosity strongly correlates with elastic modulus, as illustrated in Figure 6(b). As porosity increases, the elastic modulus decreases. A similar conclusion was made in previous literature [31,53]. Rezabeigi *et al.,* [54] reported that an increase in the porosity of the PLA foam from 40.7% to 90.8% decreased the compressive elastic modulus from 57 MPa to 1.8 MPa. Maharjan *et al.,* [55] investigated the mechanical properties of fused deposition modelling-printed gyroid PLA cellular lattices with a gyroid structure with porosity ranging from 75% to 85%. Their scaffolds exhibited an elastic modulus of over 20–76 MPa and a yield strength of 1 MPa to 3 MPa. In this study, the compressive elastic modulus and yield strength of the PLA NSP scaffold with porosity from 25% to 75% were 101,99–674,87 and 1,76–17,36 MPa, respectively. For relatively low porosity scaffolds, simulated compressive modulus values are consistent with the experimental values. For higher porosity scaffold, simulated compressive modulus values are lower than the experimental ones with a percentage difference of 10.4%, and the simulation results follow the experimental trend. The FEA findings and the experiment results are in good agreement, despite the fact the error deviation between the two outcomes. A significant enhancement of the yield strength and elastic modulus of NSP PLA scaffolds manufactured compared with the other scaffolds with similar porosity reported in the literature. The greater mechanical properties of the NSP PLA scaffold manufactured are attributable to the appropriate design parameters, including shape, porosity, pore size and

tortuosity. The tortuosity parameters contribute to enhancing the mechanical properties of the NSP scaffold. Figure 6(c) shows the correlation between tortuosity and elastic modulus of the NSP scaffold with the same porosity of 60%. The NSP 0.8, NSP 0.9 and NSP 0.98 samples generated tortuosity values of 1.8, 1.6 and 1,5, respectively. The tortuosity can be maintained within the same porosity by altering the pore size and radius of curvature. The pore size must be reduced to increase tortuosity. A relatively low pore size generated a high strut, increasing the elastic modulus. The advantage of NSP scaffold design is that it is a simple method using parametric equations and is not as difficult as TPMS, which is described using the advantages of mathematical equations [56]. Furthermore, the elastic modulus of the NSP 3D-printed scaffold is suitable for cancellous bone replacement. Fatihhi *et al.,* [57] reported a 621 MPa elastic modulus value for bovine cancellous bone with 77% density. Kopperdahl and Keaveny [58] on the contrary, reported a lower value of 291 MPa for human trabecular bone with an average density of 46% [58]. Another study reported that the elastic modulus value of natural cancellous bone is 0.01 GPa to 2 GPa, according to the anatomical site [17-19]. Additionally, the compressive properties of the PLA scaffold compared in this study and previous literature can be summarized in Table 3.

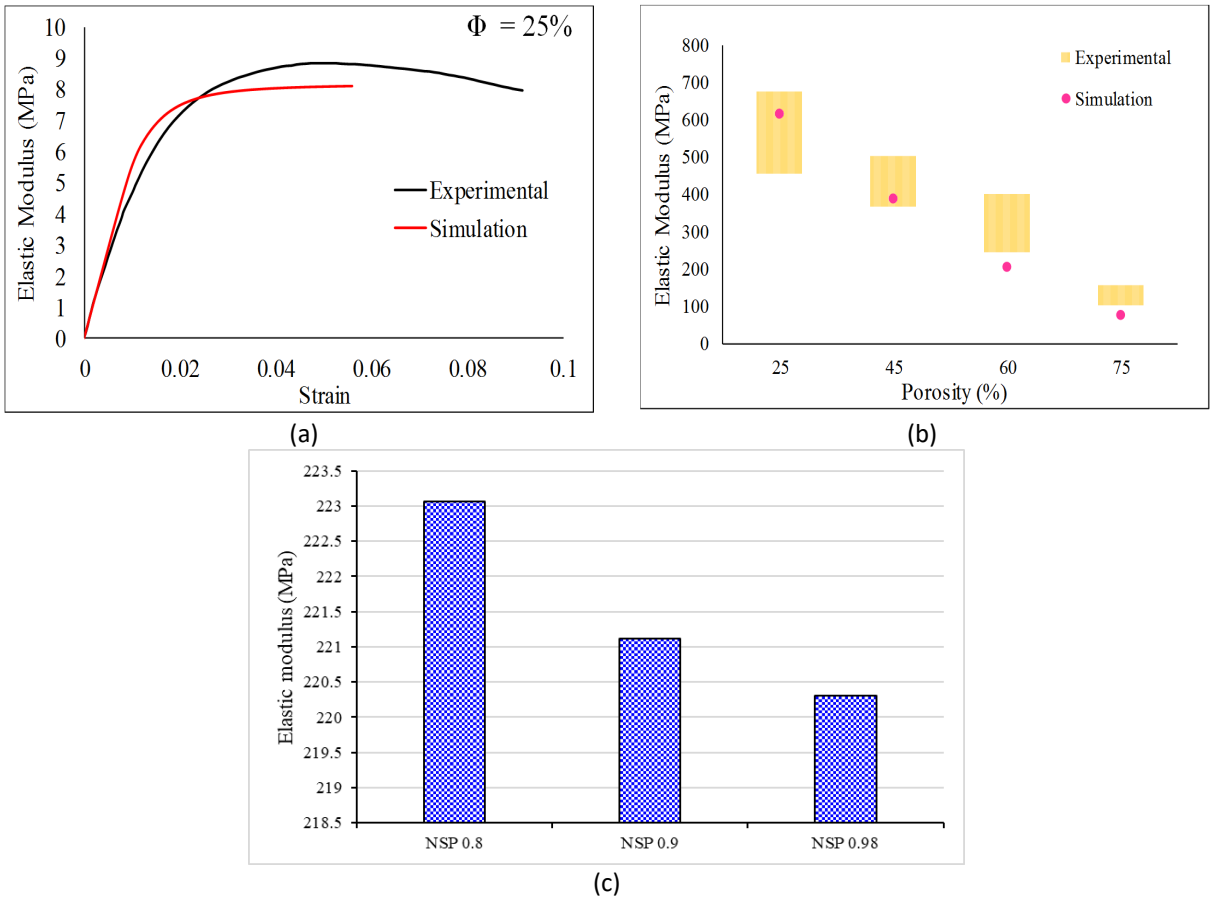

Fig. 6. (a) Comparison of compressive stress–strain curves between the experimental and finite element simulation for specimen Φ: 25%; (b) Range of modulus experimental values for specimens 25%, 45%, 60% and 75% of porosity was as follows (453.33–674.87 MPa), (367.91–503.84 MPa), (245.10–399.24 MPa) and (101.99–156.68 MPa), respectively, compare with simulation; and (c) Relationship between elastic modulus and tortuosity of NSP scaffold model with the same porosity of 60%

Table 3
Compressive properties of PLA scaffolds manufactured via fused deposition modelling in this study in comparison with various porous structures published in the literature

Scaffold	Porosity (%)	Elastic modulus, (MPa)	Yield Strength (MPa)	Method
NSP	25	545,21± 109,76	17,36 ± 4,75	Fused Desposition Modelling
NSP	45	446,82 ± 57,12	7,99 ± 2,71	Fused Desposition Modelling
NSP	60	312,55 ± 82,64	5,29 ± 1,72	Fused Desposition Modelling
NSP	75	123,81 ± 23,95	1,76 ± 1,04	Fused Desposition Modelling
Gyroid	70-75	50	-	Fused Desposition Modelling [59]
Cubic	55	0,53 ± 0,1	13,25± 1,6	Fused Desposition Modelling [60]
	60	0,40 ± 0,006	9,47± 0,47	
	66	0,46 ± 0,06	5,75± 0,27	
Grid 2xOrtho	30	818.7	22.80	Fused Desposition Modelling [46]
	50	510,81	12.89	
	70	230,49	5.31	
Grid 2xIso	30	736,43	20.17	
	50	435.75	10.72	
	70	185.96	4.21	
Bovine Cancellous bone	5.68 – 77.69	4.39-80.14	0.68-9.93	[61]

3.3 Morphology Characterization of Porous Scaffold

The macroscopic and microscopic morphology of the scaffold for the sample with Φ:60% porosity was observed using SEM, as shown in Figure 7(a). The figure shows that all pores were open, and excellent interconnection between pores was observed. In the novel NSP scaffold structure, the struts extend horizontally vertically, at an angle of 45°, and develop arc-shaped struts. Combining these struts could increase the mechanical strength of the scaffold structure. Interestingly, the structure creates a radius connection at these strut nodes and finally develops negative concave surface curvature. Scaffolds with concave surfaces can induce an earlier and quantitatively enhanced bone differentiation, as reported in previous studies [62-65]. Figure 6(b) shows the SEM images of a 3D-printed scaffold, indicating the layer-by-layer deposition of the fused PLA filaments around the pore walls. The 3D-printed layers have a smooth surface despite unattached tiny molten filament pieces. No gaps, voids or looseness between the molten PLA layers were detected despite the highly porous structure of the component. Figure 6(c) compares the scaffold structure between CAD and 3D-printed models. The strut size of the manufactured scaffolds was increased compared with the design values, and the percentage difference was below 9.93%. The strut thickness can increase the modulus stiffness of the scaffold. As the thickness of the scaffold increases, the stiffness also increases. Thus, the experiment's elastic modulus did not agree with the simulation result because of the effect of printing parameters on part accuracy [66].

The effectiveness of 3D printing techniques in generating components with complex geometries has been demonstrated. Applying suitable values of manufacturing parameters, such as speed of printing and extruder temperature, will lead to strong adhesion between the internal melted layers and achieve high-strength scaffolds. In the study of Baptista and Guedes [31,46], 0.4 mm nozzle was used at 215 °C, the printing speed was 30 mm/s, whereas the travel speed of the printer head was set to 90 mm/s to manufacture PLA scaffolds using grid model. Zarei *et al.,* [67] used a 0.4 mm nozzle

at 215 °C temperature, printing speed of 10 mm/s and 0.3 mm layer height to fabricate a grid scaffold. Osgouei *et al.,* [53] used a 0.6 mm nozzle at a 195 °C layer and height of 0.2 mm to fabricate a TPMS scaffold. Hussein *et al.,* [38] fabricated a PLA conical-graded structure using a 0.3 mm nozzle diameter, extruder temperature of 200 °C and a layer height of 0.16 mm. Although previous studies justified that the effect of design variation on mechanical properties does not depend on the scaffold scale size due to the limitations of the FDM machine, the morphology of the scaffold, such as pore size and strut thickness, must be considered to support bone regeneration. The pore size of the scaffold to support bone regeneration is approximately 500–1000 microns [68]. Printing parameters were considered effective in achieving high-quality scaffold samples, including nozzle size, extruder speed and temperature, printing speed, layer height and infilling density. High-setting parameter processing, such as 0.2 mm for nozzle size, 25 mm/s for printing speed, 210 °C for extruder temperature, 0.08 mm for layer height and 100% for infilling percentage, was selected. Therefore, selecting a set of appropriate printing parameters can be considered the key condition for achieving excellent mechanical properties of the manufactured PLA scaffold.

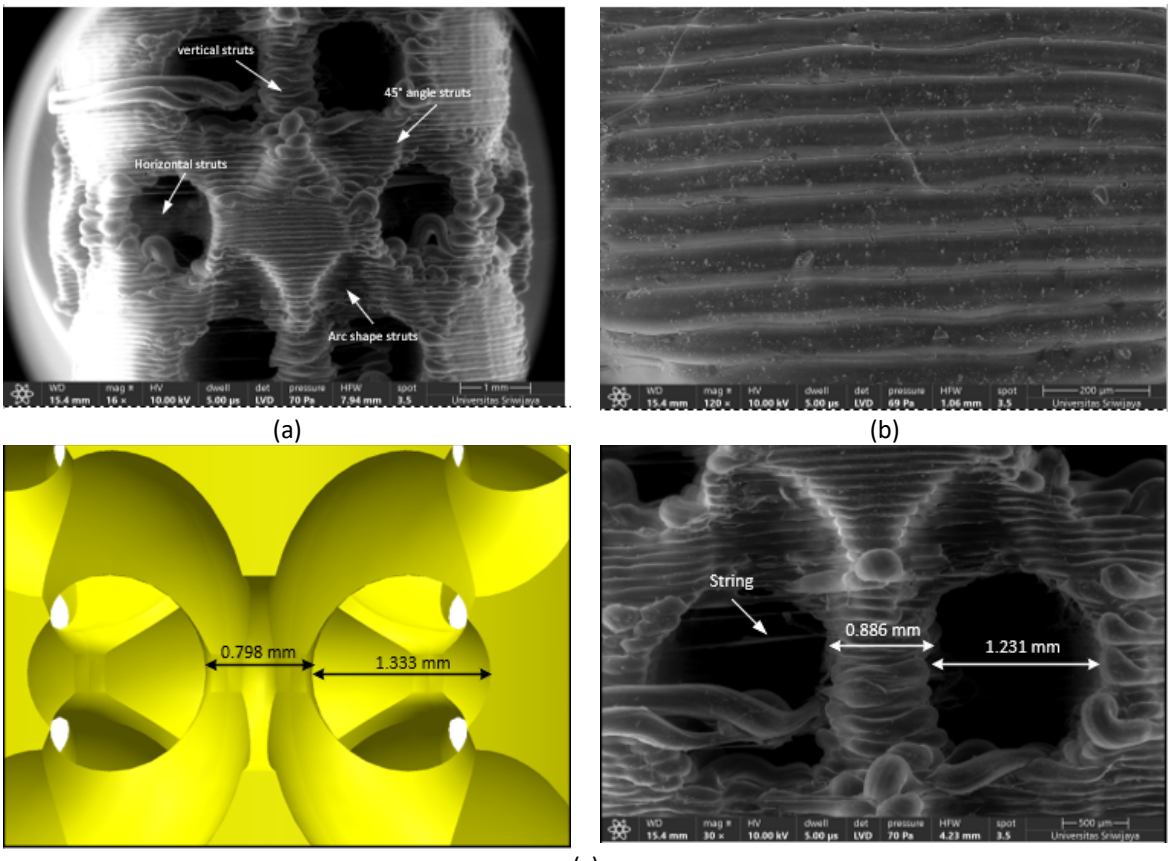

Fig. 7. (a) Morphology of scaffold model; (b) layer height; and (c) Comparison between the scaffold CAD model and printed models

3.4 Fracture Behaviour

In Figure 8, the fracture patterns and principal elastic strain of specimens with varying porosity percentages are presented under uniaxial compression tests. Specimen Φ: 45% exhibited a global fracture initiating from the middle region, whereas specimens Φ: 60% and Φ: 75% underwent global fractures commencing from the bottom region. The early failure from the bottom region can be attributed to two primary factors. Firstly, cracks typically initiate from the thinnest struts due to an

increase in pore size, and plastification progresses to form a collapse band as it traverses weak regions randomly. Secondly, the process of duplicating the unit cell into the cylindrical model contributed to a partial loss of struts. Comparisons between experimental results and predictions from FEA were made within the same group of specimen morphologies. The elastic strain indicated a similar collapsing pattern, as denoted by the black arrow, particularly when dependent on weak material struts. This information holds paramount significance in the application of bone scaffolds for load-bearing purposes. The fracture characteristics closely resemble those of actual cancellous bone, thereby representing the scaffold's damage behaviour once implanted to mitigate directional stress effects. Moreover, studies affirm that most cancellous bones generally exhibit a global fracture pattern.

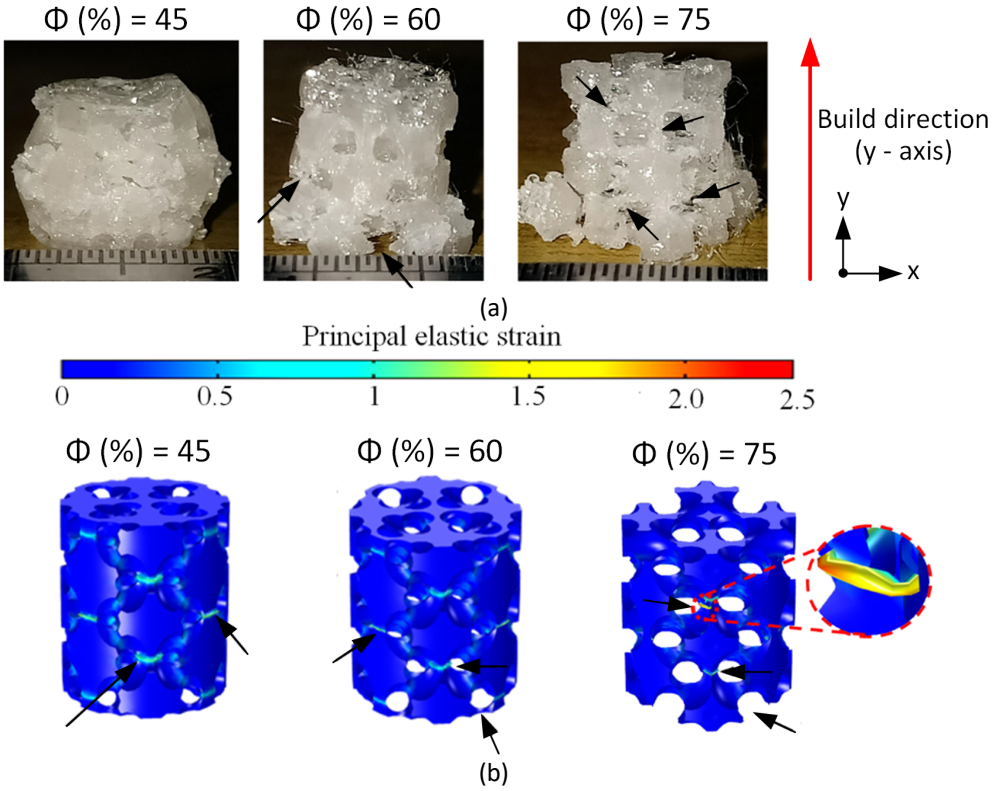

Fig. 8. (a) Contour plots of the fracture pattern under compression loading and (b) principal plastic strain contours from FEA

4. Conclusions

This study successfully introduces a novel scaffold structure design, employing a parametric approach to achieve controllable tortuosity and create surface curvature, thereby fostering an environment conducive to bone regeneration. The research significantly advances the scaffold design for bone regeneration by highlighting the crucial role of tortuosity and microarchitecture in scaffold performance. The key findings of the study are summarised as follows. Firstly, the fabrication of the scaffold using low-cost fused deposition modelling (FDM) with optimised processing parameters results in high-quality printing, effectively producing scaffolds with pore sizes suitable for bone tissue engineering. Secondly, all fabricated scaffolds exhibit elastic modulus values comparable to natural cancellous bones, ranging from 545.21 ± 109.76 MPa to 123.81 ± 23.95 MPa, corresponding to porosities of 25%, 45%, 60% and 75%. These values fall within the elastic modulus range of natural cancellous bone. Thirdly, the tortuosity parameter demonstrates a positive correlation with elastic

modulus, as indicated by a linear regression R^2 = 0.94, further emphasising the importance of tortuosity in scaffold design for optimal bone regeneration. These findings collectively contribute novel insights to scaffold design, presenting a promising avenue for enhancing bone regeneration strategies.

Acknowledgement
The authors would like to convey their great appreciation to Universitas Sriwijaya for supporting this research.

References

[1] Nguyen, Duong T., and Karen J. L. Burg. "Bone tissue engineering and regenerative medicine: Targeting pathological fractures." *Journal of Biomedical Materials Research Part A* 103, no. 1 (2015): 420-429. https://doi.org/10.1002/jbm.a.35139

[2] Bigham, Ashkan, Amir Hamed Aghajanian, Ahmad Saudi, and Mohammad Rafienia. "Hierarchical porous Mg_2SiO_4-$CoFe_2O_4$ nanomagnetic scaffold for bone cancer therapy and regeneration: surface modification and in vitro studies." *Materials Science and Engineering: C* 109 (2020): 110579. https://doi.org/10.1016/j.msec.2019.110579

[3] Kane, Robert J., Holly E. Weiss-Bilka, Matthew J. Meagher, Yongxing Liu, Joshua A. Gargac, Glen L. Niebur, Diane R. Wagner, and Ryan K. Roeder. "Hydroxyapatite reinforced collagen scaffolds with improved architecture and mechanical properties." *Acta Biomaterialia* 17 (2015): 16-25. https://doi.org/10.1016/j.actbio.2015.01.031

[4] Giannoudis, Peter V., Haralambos Dinopoulos, and Eleftherios Tsiridis. "Bone substitutes: an update." *Injury* 36, no. 3 (2005): S20-S27. https://doi.org/10.1016/j.injury.2005.07.029

[5] Sarkar, Michael R., Peter Augat, Sandra J. Shefelbine, Sandra Schorlemmer, Markus Huber-Lang, Lutz Claes, Lothar Kinzl, and Anita Ignatius. "Bone formation in a long bone defect model using a platelet-rich plasma-loaded collagen scaffold." *Biomaterials* 27, no. 9 (2006): 1817-1823. https://doi.org/10.1016/j.biomaterials.2005.10.039

[6] Liu, Fei, Zhongfa Mao, Peng Zhang, David Z. Zhang, Junjie Jiang, and Zhibo Ma. "Functionally graded porous scaffolds in multiple patterns: New design method, physical and mechanical properties." *Materials & Design* 160 (2018): 849-860. https://doi.org/10.1016/j.matdes.2018.09.053

[7] Giannitelli, Sara Maria, Dino Accoto, Marcella Trombetta, and Alberto Rainer. "Current trends in the design of scaffolds for computer-aided tissue engineering." *Acta Biomaterialia* 10, no. 2 (2014): 580-594. https://doi.org/10.1016/j.actbio.2013.10.024

[8] Zhang, Xiang-Yu, Gang Fang, and Jie Zhou. "Additively manufactured scaffolds for bone tissue engineering and the prediction of their mechanical behavior: A review." *Materials* 10, no. 1 (2017): 50. https://doi.org/10.3390/ma10010050

[9] Prakoso, Akbar Teguh, Hasan Basri, Dendy Adanta, Irsyadi Yani, Muhammad Imam Ammarullah, Imam Akbar, Farah Amira Ghazali, Ardiyansyah Syahrom, and Tunku Kamarul. "The effect of tortuosity on permeability of porous scaffold." *Biomedicines* 11, no. 2 (2023): 427. https://doi.org/10.3390/biomedicines11020427

[10] Ali, Davar. "Effect of scaffold architecture on cell seeding efficiency: A discrete phase model CFD analysis." *Computers in Biology and Medicine* 109 (2019): 62-69. https://doi.org/10.1016/j.compbiomed.2019.04.025

[11] Kuboki, Y., H. Takita, D. Kobayashi, E. Tsuruga, M. Inoue, M. Murata, N. Nagai, Y. Dohi, and H. Ohgushi. "BMP-induced osteogenesis on the surface of hydroxyapatite with geometrically feasible and nonfeasible structures: topology of osteogenesis." *Journal of Biomedical Materials Research: An Official Journal of The Society for Biomaterials, The Japanese Society for Biomaterials, and the Australian Society for Biomaterials* 39, no. 2 (1998): 190-199. https://doi.org/10.1002/(SICI)1097-4636(199802)39:2<190::AID-JBM4>3.0.CO;2-K

[12] Arifin, Amir, Gunawan, M. Wahyudi Amin, Alim Mardhi, Ganang Trycahyono, and Firmansyah Burlian. "Characterization Porous HA/SiO2 Composite Prepared Using Natural Space Holder." In *Human-Centered Technology for a Better Tomorrow: Proceedings of HUMENS 2021*, pp. 279-287. Springer Singapore, 2022. https://doi.org/10.1007/978-981-16-4115-2_22

[13] Arifin, Amir, Irsyadi Yani, and Sufran Danar Arian. "The fabrication porous hydroxyapatite scaffold using sweet potato starch as a natural space holder." In *Journal of Physics: Conference Series*, vol. 1198, no. 4, p. 042020. IOP Publishing, 2019. https://doi.org/10.1088/1742-6596/1198/4/042020

[14] Engh, Charles A., J. Dennis Bobyn, and Andrew H. Glassman. "Porous-coated hip replacement. The factors governing bone ingrowth, stress shielding, and clinical results." *The Journal of Bone & Joint Surgery British Volume* 69, no. 1 (1987): 45-55. https://doi.org/10.1302/0301-620X.69B1.3818732

[15] Arifin, Amir, Abu Bakar Sulong, Norhamidi Muhamad, Junaidi Syarif, and Mohd Ikram Ramli. "Material processing of hydroxyapatite and titanium alloy (HA/Ti) composite as implant materials using powder metallurgy: A review."

Materials & Design 55 (2014): 165-175. https://doi.org/10.1016/j.matdes.2013.09.045
[16] Arifin, Amir, Abu Bakar Sulong, Norhamidi Muhamad, Junaidi Syarif, and Mohd Ikram Ramli. "Powder injection molding of HA/Ti_6Al_4V composite using palm stearin as based binder for implant material." *Materials & Design (1980-2015)* 65 (2015): 1028-1034. https://doi.org/10.1016/j.matdes.2014.10.039
[17] Saad, Amir Putra Md, Noor Jasmawati, Muhamad Noor Harun, Mohammed Rafiq Abdul Kadir, Hadi Nur, Hendra Hermawan, and Ardiyansyah Syahrom. "Dynamic degradation of porous magnesium under a simulated environment of human cancellous bone." *Corrosion Science* 112 (2016): 495-506. https://doi.org/10.1016/j.corsci.2016.08.017
[18] Karageorgiou, Vassilis, and David Kaplan. "Porosity of 3D biomaterial scaffolds and osteogenesis." *Biomaterials* 26, no. 27 (2005): 5474-5491. https://doi.org/10.1016/j.biomaterials.2005.02.002
[19] Fernandes, Cristiana, Carla Moura, Rita MT Ascenso, Sandra Amado, Nuno Alves, and Paula Pascoal-Faria. "Comprehensive review on full bone regeneration through 3D printing approaches." *Design and Manufacturing* (2020). https://doi.org/10.5772/intechopen.90864
[20] Tang, Daniel, Rahul S. Tare, Liang-Yo Yang, David F. Williams, Keng-Liang Ou, and Richard O. C. Oreffo. "Biofabrication of bone tissue: approaches, challenges and translation for bone regeneration." *Biomaterials* 83 (2016): 363-382. https://doi.org/10.1016/j.biomaterials.2016.01.024
[21] Abdulhameed, Osama, Abdulrahman Al-Ahmari, Wadea Ameen, and Syed Hammad Mian. "Additive manufacturing: Challenges, trends, and applications." *Advances in Mechanical Engineering* 11, no. 2 (2019): 1687814018822880. https://doi.org/10.1177/1687814018822880
[22] Solomon, I. John, P. Sevvel, and J. J. M. T. P. Gunasekaran. "A review on the various processing parameters in FDM." *Materials Today: Proceedings* 37 (2021): 509-514. https://doi.org/10.1016/j.matpr.2020.05.484
[23] Calignano, Flaviana, Manuela Galati, Luca Iuliano, and Paolo Minetola. "Design of additively manufactured structures for biomedical applications: a review of the additive manufacturing processes applied to the biomedical sector." *Journal of Healthcare Engineering* 2019 (2019). https://doi.org/10.1155/2019/9748212
[24] Ramot, Yuval, Moran Haim-Zada, Abraham J. Domb, and Abraham Nyska. "Biocompatibility and safety of PLA and its copolymers." Advanced Drug Delivery Reviews 107 (2016): 153-162. https://doi.org/10.1016/j.addr.2016.03.012
[25] Middleton, John C., and Arthur J. Tipton. "Synthetic biodegradable polymers as orthopedic devices." *Biomaterials* 21, no. 23 (2000): 2335-2346. https://doi.org/10.1016/S0142-9612(00)00101-0
[26] Singh, Daljeet, Atul Babbar, Vivek Jain, Dheeraj Gupta, Sanjai Saxena, and Vagish Dwibedi. "Synthesis, characterization, and bioactivity investigation of biomimetic biodegradable PLA scaffold fabricated by fused filament fabrication process." *Journal of the Brazilian Society of Mechanical Sciences and Engineering* 41 (2019): 1-13. https://doi.org/10.1007/s40430-019-1625-y
[27] Domingos, M., F. Intranuovo, T. Russo, R. De Santis, A. Gloria, L. Ambrosio, J. Ciurana, and P. Bartolo. "The first systematic analysis of 3D rapid prototyped poly (ε-caprolactone) scaffolds manufactured through BioCell printing: the effect of pore size and geometry on compressive mechanical behaviour and in vitro hMSC viability." *Biofabrication* 5, no. 4 (2013): 045004. https://doi.org/10.1088/1758-5082/5/4/045004
[28] Zein, Iwan, Dietmar W. Hutmacher, Kim Cheng Tan, and Swee Hin Teoh. "Fused deposition modeling of novel scaffold architectures for tissue engineering applications." *Biomaterials* 23, no. 4 (2002): 1169-1185. https://doi.org/10.1016/S0142-9612(01)00232-0
[29] Gleadall, Andrew, Dafydd Visscher, Jing Yang, Daniel Thomas, and Joel Segal. "Review of additive manufactured tissue engineering scaffolds: relationship between geometry and performance." *Burns & Trauma* 6 (2018). https://doi.org/10.1186/s41038-018-0121-4
[30] Serra, Tiziano, Josep A. Planell, and Melba Navarro. "High-resolution PLA-based composite scaffolds via 3-D printing technology." *Acta Biomaterialia* 9, no. 3 (2013): 5521-5530. https://doi.org/10.1016/j.actbio.2012.10.041
[31] Baptista, R., and M. Guedes. "Morphological and mechanical characterization of 3D printed PLA scaffolds with controlled porosity for trabecular bone tissue replacement." *Materials Science and Engineering: C* 118 (2021): 111528. https://doi.org/10.1016/j.msec.2020.111528
[32] Lee, Se-Hwan, Kang-Gon Lee, Jong-Hyun Hwang, Yong Sang Cho, Kang-Sik Lee, Hun-Jin Jeong, Sang-Hyug Park, Yongdoo Park, Young-Sam Cho, and Bu-Kyu Lee. "Evaluation of mechanical strength and bone regeneration ability of 3D printed kagome-structure scaffold using rabbit calvarial defect model." *Materials Science and Engineering: C* 98 (2019): 949-959. https://doi.org/10.1016/j.msec.2019.01.050
[33] Xie, Chaoqi, Qing Gao, Peng Wang, Lei Shao, Huipu Yuan, Jianzhong Fu, Wei Chen, and Yong He. "Structure-induced cell growth by 3D printing of heterogeneous scaffolds with ultrafine fibers." *Materials & Design* 181 (2019): 108092. https://doi.org/10.1016/j.matdes.2019.108092
[34] Reyes, Rigoberto Lopez, Min-Soo Ghim, Nae-Un Kang, Ji-Woo Park, So-Jung Gwak, and Young-Sam Cho. "Development and assessment of modified-honeycomb-structure scaffold for bone tissue engineering." *Additive Manufacturing* 54 (2022): 102740. https://doi.org/10.1016/j.addma.2022.102740

[35] Karimipour-Fard, Pedram, Amir H. Behravesh, Holly Jones-Taggart, Remon Pop-Iliev, and Ghaus Rizvi. "Effects of design, porosity and biodegradation on mechanical and morphological properties of additive-manufactured triply periodic minimal surface scaffolds." *Journal of the Mechanical Behavior of Biomedical Materials* 112 (2020): 104064. https://doi.org/10.1016/j.jmbbm.2020.104064

[36] Zhianmanesh, Masoud, Mostafa Varmazyar, and Hossein Montazerian. "Fluid permeability of graded porosity scaffolds architectured with minimal surfaces." *ACS Biomaterials Science & Engineering* 5, no. 3 (2019): 1228-1237. https://doi.org/10.1021/acsbiomaterials.8b01400

[37] Castro, A. P. G., T. Pires, J. E. Santos, B. P. Gouveia, and P. R. Fernandes. "Permeability versus design in TPMS scaffolds." *Materials* 12, no. 8 (2019): 1313. https://doi.org/10.3390/ma12081313

[38] Hussein, Nur Aqila Kadir, Muhammad Azfar Noordin, and Amir Putra Md Saad. "Influence of conical graded porous architecture on the mechanical, failure behavior and fluid-flow properties for bone scaffold application." *Engineering Failure Analysis* 157 (2024): 107893. https://doi.org/10.1016/j.engfailanal.2023.107893

[39] Syahrom, Ardiyansyah, Mohammed Rafiq Abdul Kadir, Jaafar Abdullah, and Andreas Öchsner. "Permeability studies of artificial and natural cancellous bone structures." *Medical Engineering & Physics* 35, no. 6 (2013): 792-799. https://doi.org/10.1016/j.medengphy.2012.08.011

[40] Bidan, Cécile M., Krishna P. Kommareddy, Monika Rumpler, Philip Kollmannsberger, Peter Fratzl, and John WC Dunlop. "Geometry as a factor for tissue growth: towards shape optimization of tissue engineering scaffolds." *Advanced Healthcare Materials* 2, no. 1 (2013): 186-194. https://doi.org/10.1002/adhm.201200159

[41] Mazalan, Mazlee Bin, Mohamad Anis Bin Ramlan, Jennifer Hyunjong Shin, and Toshiro Ohashi. "Effect of geometric curvature on collective cell migration in tortuous microchannel devices." *Micromachines* 11, no. 7 (2020): 659. https://doi.org/10.3390/mi11070659

[42] Polo-Corrales, Liliana, Magda Latorre-Esteves, and Jaime E. Ramirez-Vick. "Scaffold design for bone regeneration." *Journal of Nanoscience and Nanotechnology* 14, no. 1 (2014): 15-56. https://doi.org/10.1166/jnn.2014.9127

[43] Rouwkema, Jeroen, Nicolas C. Rivron, and Clemens A. van Blitterswijk. "Vascularization in tissue engineering." *Trends in Biotechnology* 26, no. 8 (2008): 434-441. https://doi.org/10.1016/j.tibtech.2008.04.009

[44] Cooper, Samuel J., Antonio Bertei, Paul R. Shearing, J. A. Kilner, and Nigel P. Brandon. "TauFactor: An open-source application for calculating tortuosity factors from tomographic data." *SoftwareX* 5 (2016): 203-210. https://doi.org/10.1016/j.softx.2016.09.002

[45] Fu, Jinlong, Hywel R. Thomas, and Chenfeng Li. "Tortuosity of porous media: Image analysis and physical simulation." *Earth-Science Reviews* 212 (2021): 103439. https://doi.org/10.1016/j.earscirev.2020.103439

[46] Baptista, R., and M. Guedes. "Porosity and pore design influence on fatigue behavior of 3D printed scaffolds for trabecular bone replacement." *Journal of the Mechanical Behavior of Biomedical Materials* 117 (2021): 104378. https://doi.org/10.1016/j.jmbbm.2021.104378

[47] Abidin, Zainal, M. Yanis, M. Zahri Kadir, Akbar Teguh Prakoso, Edo Syahrizal, Ardiyansyah Syahrom, and Hasan Basri. "Optimization of FDM 3D Printing Process Parameter for Improving Porosity Accuracy of PLA Scaffold." In *4th Forum in Research, Science, and Technology (FIRST-T1-T2-2020)*, pp. 155-161. Atlantis Press, 2021. https://doi.org/10.2991/ahe.k.210205.028

[48] Zhang, Bin, Liwei Guo, Hongyi Chen, Yiannis Ventikos, Roger J. Narayan, and Jie Huang. "Finite element evaluations of the mechanical properties of polycaprolactone/hydroxyapatite scaffolds by direct ink writing: Effects of pore geometry." *Journal of the Mechanical Behavior of Biomedical Materials* 104 (2020): 103665. https://doi.org/10.1016/j.jmbbm.2020.103665

[49] Adanta, Dendy, Mochammad Malik Ibrahim, Dewi Puspita Sari, Imam Syofii, and Muhammad Amsal Ade Saputra. "Application of the grid convergency index method and courant number analysis for propeller turbine simulation." *Journal of Advanced Research in Fluid Mechanics and Thermal Sciences* 96, no. 2 (2022): 33-41. https://doi.org/10.37934/arfmts.96.2.3341

[50] Sun, Q., G. M. Rizvi, C. T. Bellehumeur, and P. Gu. "Effect of processing conditions on the bonding quality of FDM polymer filaments." *Rapid Prototyping Journal* 14, no. 2 (2008): 72-80. https://doi.org/10.1108/13552540810862028

[51] Chacón, Jesus Miguel, Miguel Angel Caminero, Eustaquio García-Plaza, and Pedro J. Núnez. "Additive manufacturing of PLA structures using fused deposition modelling: Effect of process parameters on mechanical properties and their optimal selection." *Materials & Design* 124 (2017): 143-157. https://doi.org/10.1016/j.matdes.2017.03.065

[52] Mohamed, Omar A., Syed H. Masood, and Jahar L. Bhowmik. "Optimization of fused deposition modeling process parameters: a review of current research and future prospects." *Advances in Manufacturing* 3 (2015): 42-53. https://doi.org/10.1007/s40436-014-0097-7

[53] Osgouei, Mona Alizadeh, Yuncang Li, Alireza Vahid, Arash Ataee, and Cuie Wen. "High strength porous PLA gyroid scaffolds manufactured via fused deposition modeling for tissue-engineering applications." *Smart Materials in*

Medicine 2 (2021): 15-25. https://doi.org/10.1016/j.smaim.2020.10.003
[54] Rezabeigi, Ehsan, Paula M. Wood-Adams, and Robin AL Drew. "Production of porous polylactic acid monoliths via nonsolvent induced phase separation." *Polymer* 55, no. 26 (2014): 6743-6753. https://doi.org/10.1016/j.polymer.2014.10.063
[55] Maharjan, Gopal K., Sohaib Z. Khan, Syed H. Riza, and S. H. Masood. "Compressive behaviour of 3D printed polymeric gyroid cellular lattice structure." In *IOP Conference Series: Materials Science and Engineering*, vol. 455, p. 012047. IOP Publishing, 2018. https://doi.org/10.1088/1757-899X/455/1/012047
[56] Lu, Jiaxiong, Peng Dong, Yongtao Zhao, Yan Zhao, and Yong Zeng. "3D printing of TPMS structural ZnO ceramics with good mechanical properties." *Ceramics International* 47, no. 9 (2021): 12897-12905. https://doi.org/10.1016/j.ceramint.2021.01.152
[57] Fatihhi, S. J., A. A. R. Rabiatul, M. N. Harun, Mohammed Rafiq Abdul Kadir, T. Kamarul, and Ardiyansyah Syahrom. "Effect of torsional loading on compressive fatigue behaviour of trabecular bone." *Journal of the Mechanical Behavior of Biomedical Materials* 54 (2016): 21-32. https://doi.org/10.1016/j.jmbbm.2015.09.006
[58] Kopperdahl, David L., and Tony M. Keaveny. "Yield strain behavior of trabecular bone." *Journal of Biomechanics* 31, no. 7 (1998): 601-608. https://doi.org/10.1016/S0021-9290(98)00057-8
[59] Germain, Loïc, Carlos A. Fuentes, Aart W. van Vuure, Anne des Rieux, and Christine Dupont-Gillain. "3D-printed biodegradable gyroid scaffolds for tissue engineering applications." *Materials & Design* 151 (2018): 113-122. https://doi.org/10.1016/j.matdes.2018.04.037
[60] Teixeira, B., Marianna OC Maia-Pinto, Mônica D. Calasans-Maia, Daniel J. Kelly, and R. M. S. M. Thiré. "Structural evaluation of PLA scaffolds obtained by 3D printing via fused deposition modeling (FDM) technique for applications in tissue engineering." In *Proceedings of the 5◦ Edição do Workshop de Biomateriais, Engenharia de Tecidos e Orgãos Artificiais*, Maresias, SP, Brazil, pp. 20-24. 2017. https://doi.org/10.3389/conf.FBIOE.2016.01.00092
[61] Syahrom, Ardiyansyah, Mohammed Rafiq Abdul Kadir, Jaafar Abdullah, and Andreas Öchsner. "Mechanical and microarchitectural analyses of cancellous bone through experiment and computer simulation." *Medical & Biological Engineering & Computing* 49 (2011): 1393-1403. https://doi.org/10.1007/s11517-011-0833-0
[62] Graziano, Antonio, Riccardo d'Aquino, Maria Gabriella Cusella-De Angelis, Francesco De Francesco, Antonio Giordano, Gregorio Laino, Adriano Piattelli, Tonino Traini, Alfredo De Rosa, and Gianpaolo Papaccio. "Scaffold's surface geometry significantly affects human stem cell bone tissue engineering." *Journal of Cellular Physiology* 214, no. 1 (2008): 166-172. https://doi.org/10.1002/jcp.21175
[63] Rumpler, Monika, Alexander Woesz, John W. C. Dunlop, Joost T. Van Dongen, and Peter Fratzl. "The effect of geometry on three-dimensional tissue growth." *Journal of the Royal Society Interface* 5, no. 27 (2008): 1173-1180. https://doi.org/10.1098/rsif.2008.0064
[64] Zhang, Yun, Peng Wang, Jiyong Jin, Lan Li, Si-yuan He, Ping Zhou, Qing Jiang, and Cuie Wen. "In silico and in vivo studies of the effect of surface curvature on the osteoconduction of porous scaffolds." *Biotechnology and Bioengineering* 119, no. 2 (2022): 591-604. https://doi.org/10.1002/bit.27976
[65] Li, Zhitong, Zhaobo Chen, Xiongbiao Chen, and Runchao Zhao. "Effect of surface curvature on the mechanical and mass-transport properties of additively manufactured tissue scaffolds with minimal surfaces." *ACS Biomaterials Science & Engineering* 8, no. 4 (2022): 1623-1643. https://doi.org/10.1021/acsbiomaterials.1c01438
[66] Dong, Guoying, Grace Wijaya, Yunlong Tang, and Yaoyao Fiona Zhao. "Optimizing process parameters of fused deposition modeling by Taguchi method for the fabrication of lattice structures." *Additive Manufacturing* 19 (2018): 62-72. https://doi.org/10.1016/j.addma.2017.11.004
[67] Zarei, Masoud, Mohammad Mahdi Hosseini Nikoo, Reza Alizadeh, and Amirhossein Askarinya. "Synergistic effect of $CaCO_3$ addition and in-process cold atmospheric plasma treatment on the surface evolution, mechanical properties, and in-vitro degradation behavior of FDM-printed PLA scaffolds." *Journal of the Mechanical Behavior of Biomedical Materials* 149 (2024): 106239. https://doi.org/10.1016/j.jmbbm.2023.106239
[68] Kim, Eun-Jin, So-Young Bu, Mi-Kyung Sung, and Mi-Kyeong Choi. "Effects of silicon on osteoblast activity and bone mineralization of MC3T3-E1 cells." *Biological Trace Element Research* 152 (2013): 105-112. https://doi.org/10.1007/s12011-012-9593-4